1    **Arctic Ocean CO₂ uptake: an improved multi-year estimate of the air–sea CO₂ flux**

2    **incorporating chlorophyll-a concentrations**

4    Sayaka Yasunaka[1,2], Eko Siswanto[1], Are Olsen[3], Mario Hoppema[4], Eiji Watanabe[2],

5    Agneta Fransson[5], Melissa Chierici[6], Akihiko Murata[1,2], Siv K. Lauvset[4,7], Rik

6    Wanninkhof[8], Taro Takahashi[9], Naohiro Kosugi[10], Abdirahman M. Omar[7], Steven van

7    Heuven[11], and Jeremy T. Mathis[12]

9    [1]Research and Development Center for Global Change, Japan Agency for Marine-Earth

10    Science and Technology, Yokosuka, Japan

11    [2]Institute of Arctic Climate and Environment Research, Japan Agency for Marine-Earth

12    Science and Technology, Yokosuka, Japan

13    [3]Geophysical Institute, University of Bergen and Bjerknes Centre for Climate Research,

14    Bergen, Norway

15    [4]Alfred Wegener Institute Helmholtz Centre for Polar and Marine Research, Climate

16    Sciences Department, Bremerhaven, Germany

17    [5]Norwegian Polar Institute, Fram Centre, Norway

18    [6]Institute of Marine Research, Tromsø, Norway

19    [7]Uni Research Climate, Bjerknes Centre for Climate Research, Bergen, Norway

20    [8]NOAA, Atlantic Oceanographic and Meteorological Laboratory, Miami, FL, USA

21    [9]Lamont-Doherty Earth Observatory of Columbia University, Palisades, NY, USA

22    [10]Oceanography and Geochemistry Research Department, Meteorological Research

23    Institute, Japan Meteorological Agency, Tsukuba, Japan

24    [11]Energy and Sustainability Research Institute Groningen, Groningen University, The

25    Netherlands

26    [12]NOAA, Arctic Research Program, Seattle, WA, USA

28    **Abstract**

29    We estimated monthly air–sea $CO_2$ fluxes in the Arctic Ocean and its adjacent seas

30    north of 60° N from 1997 to 2014, after mapping partial pressure of $CO_2$ in the surface

31    water ($pCO_{2w}$) using a self-organizing map (SOM) technique incorporating

32    chlorophyll-a concentration (Chl-a), sea surface temperature, sea surface salinity, sea ice

33    concentration, atmospheric $CO_2$ mixing ratio, and geographical position. The overall

34    relationship between $pCO_{2w}$ and Chl-a is negative in most regions when Chl-a ≤ 1 mg

35    $m^{-3}$, whereas there is no significant relationship when Chl-a > 1 mg $m^{-3}$. In the Kara

36    Sea and the East Siberian Sea and the Bering Strait, however, the relationship is

37    typically positive in summer. The addition of Chl-a as a parameter in the SOM process

38    enabled us to improve the estimate of $p$CO$_{2w}$ via better representation of its decline in

39    spring, which resulted from biologically mediated $p$CO$_{2w}$ reduction. Mainly as a result

40    of the inclusion of Chl-a, the uncertainty in the CO$_2$ flux estimate was reduced, and a

41    net annual Arctic Ocean CO$_2$ uptake of $180 \pm 130$ TgC y$^{-1}$ was determined to be

42    significant.

44    **1. Introduction**

45    The Arctic Ocean and its adjacent seas (Fig. 1) are thought to act as a sink for

46    atmospheric CO$_2$ because of the high solubility of CO$_2$ in its low-temperature waters,

47    combined with its extensive primary production during the summer season (Bates and

48    Mathis, 2009). The Arctic Ocean and its adjacent seas consist of complicated subregions

49    that include continental shelves, central basins, and sea-ice-covered areas. Therefore,

50    the surface partial pressure of CO$_2$ ($p$CO$_{2w}$) distribution is not only affected by ocean

51    heat loss and gain, and biological production and respiration, but also by sea-ice

52    formation and melting, river discharge, and shelf–basin interactions (cf. Bates and

53    Mathis, 2009). CO$_2$ measurements are sparse in this very heterogeneous area (Fig. 2),

54    and hence air–sea CO$_2$ flux estimates in the Arctic have shown poor agreement

55    (Schuster et al., 2013).

56        As global warming progresses, melting of sea ice will increase the area of open water

57    and enhance the potential for uptake of atmospheric $CO_2$ (e.g., Bates et al., 2006; Gao et

58    al., 2012). However, other processes will occur simultaneously, some of which could

59    suppress $CO_2$ uptake. For example, increasing seawater temperatures, declining buffer

60    capacity due to the freshening of Arctic surface water by increased river runoff and

61    ice-melting, and increased vertical mixing supplying high-$CO_2$ water to the surface

62    (Bates and Mathis, 2009; Cai et al., 2010; Chierici et al., 2011; Else et al., 2013; Bates

63    et al. 2014; Fransson et al., 2017), will all result in a tendency for reduced uptake. The

64    combined effect of all these processes on ocean $CO_2$ uptake has not yet been clarified

65    for the Arctic.

66        Yasunaka et al. (2016) successfully prepared monthly maps of air–sea $CO_2$ fluxes

67    from 1997 to 2013 for the Arctic north of 60° N by applying, for the first time, a

68    self-organizing map (SOM) technique to map $p\mathrm{CO}_{2w}$ in the Arctic Ocean. The

69    advantage of the SOM technique is its ability to empirically determine relationships

70    among variables without making any a priori assumptions (e.g., what types of

71    regression functions are applicable, and for which sub-regions the same regression

72    function can be adopted). The SOM technique has been shown to reproduce the

73    distribution of $pCO_{2w}$ from unevenly distributed observations better than multiple

74    regression methods (Lefèvre et al., 2005; Telszewski et al., 2009). The uncertainty of

75    the $CO_2$ flux estimated by Yasunaka et al. (2016), however, was large (±3.4–4.6 mmol

76    $m^{-2}$ $d^{-1}$), and the estimated $CO_2$ uptake in the Arctic Ocean was smaller than the

77    uncertainty ($180 \pm 210$ TgC $y^{-1}$). One possible reason for the large uncertainties is that

78    the effect of biological processes on explaining the variability was not included among

79    the parameters used in the SOM process, which could lead to an underestimation of the

80    seasonal amplitude of $pCO_{2w}$.

81       Several studies have estimated chlorophyll-a concentrations (Chl-a) in the Arctic

82    from satellite remote sensing reflectance (Rrs) (e.g. Arrigo and Dijken, 2004; Cota et al.,

83    2004). Perrette et al. (2011) showed that satellite-derived Chl-a successfully captured a

84    phytoplankton bloom in the ice-edge region. Changes in the seasonal cycle of Chl-a

85    have also been observed and are likely a consequence of the recent sea-ice loss in the

86    Arctic (Ardyna et al., 2014). Measurements in several areas of the Arctic show that the

87    relationship between $pCO_{2w}$ and Chl-a is typically negative, as expected (Gao et al.,

88    2012; Ulfsbo et al., 2014). Exceptions do occur, however, in the coastal regions, where

89    the relationship is positive (Mucci et al., 2010). Chierici et al. (2009) produced $pCO_{2w}$

90    algorithms for the subpolar North Atlantic and found that the inclusion of Chl-a

91    improved the fit substantially during the period from May to October.

92      In the present study, we examined the relationship between $pCO_{2w}$ and Chl-a in the

93    Arctic Ocean and its adjacent seas, and presented monthly air–sea $CO_2$ flux maps for

94    regions north of 60° N using a SOM technique similar to that of Yasunaka et al. (2016),

95    and with Chl-a added to the SOM process.

96

97    **2. Data**

98    2.1. $pCO_{2\,w}$ measurements

99    We used $pCO_{2w}$ observations (converted from the fugacity of $CO_2$ values; a correction

100   of <1 %) from the Surface Ocean $CO_2$ Atlas version 4 (SOCATv4; Bakker et al., 2016;

101   http://www.socat.info/; 1,983,799 data from >60° N), and from the Global Surface

102   $pCO_2$ Database Version 2014 (LDEOv2014; Takahashi et al., 2015;

103   http://cdiac.ornl.gov/oceans/LDEO_Underway_Database/; 302,150 data from >60° N).

104   Duplicate data points were eliminated; the SOCAT versions of these duplicates were

105   used, except for the data obtained from onboard the USCGC *Healy* as these have been

106   reanalyzed by Takahashi et al. (2015). Altogether 200,409 duplicates were removed. We

107   also used shipboard $pCO_{2w}$ data obtained during cruises of the R/V *Mirai* of the Japan

108   Agency for Marine-Earth Science and Technology (JAMSTEC) that have not yet been

109     included in SOCATv4 or LDEOv2014 (cruises MR09_03, MR10_05, MR12_E03, and

110     MR13_06; http://www.godac.jamstec.go.jp/darwin/e; 95,725 data from >60° N). In total,

111     we used 2,181,265 $p$CO$_{2w}$ data, 33 % more than used by Yasunaka et al. (2016).

112     To improve the data coverage, especially for the ice-covered regions, we also used

113     2166 $p$CO$_{2w}$ values calculated from dissolved inorganic carbon and total alkalinity data

114     extracted from the Global Ocean Data Analysis Project version 2 (GLODAPv2; Key et

115     al., 2015; Olsen et al., 2016; http://cdiac.ornl.gov/oceans/GLODAPv2/). 90% of these

116     data were obtained at cruises without available underway $p$CO$_{2w}$ data. We extracted

117     values of samples obtained from water depths shallower than 10 m, or the shallowest

118     values from the upper 30 m of each cast if there were no values from above 10 m. We

119     used the CO2SYS program (Lewis and Wallace, 1998; van Heuven et al., 2009) and the

120     dissociation constants reported by Lueker et al. (2000) and Dickson (1990) for the

121     calculation. This resulted in 94 % more calculated $p$CO$_{2w}$ values than used by Yasunaka

122     et al. (2016).

123     The availability of $p$CO$_{2w}$ data (directly measured and calculated) varied spatially and

124     temporally (Fig. 2). Most of the available data are from the subpolar North Atlantic, the

125     Greenland Sea, the Norwegian Sea, the Barents Sea, and the Chukchi Sea while much

126     less data are available for the Kara Sea, the Laptev Sea, the East Siberian Sea, and the

127    Eurasian Basin. The number of $p\mathrm{CO}_{2\mathrm{w}}$ data strongly increases after 2005, but there is

128    also a substantial number of data from before 2004.

129

130    2.2. Other data

131    To calculate Chl-a, we used merged Rrs data from multi-ocean color sensors processed

132    and distributed by the GlobColour Project (Maritorena et al., 2010;

133    http://hermes.acri.fr/index.php?class=archive). For compatibility with the

134    spatio-temporal resolution of the gridded $p\mathrm{CO}_{2\mathrm{w}}$ data (see Sect. 3.3), we selected

135    monthly mean Rrs data with a spatial resolution of 1° × 1°.

136       Sea surface temperature (SST) data were extracted from the National Oceanic and

137    Atmospheric Administration (NOAA) Optimum Interpolation SST Version 2 (Reynolds

138    et al., 2002; http://www.esrl.noaa.gov/psd/data/gridded/data.noaa.oisst.v2.html). These

139    data are provided at a resolution of 1° (latitude) × 1° (longitude) × 1 month. The sea

140    surface salinity (SSS) data were retrieved from the Polar Science Center Hydrographic

141    Climatology version 3.0, which also has a resolution of 1° × 1°× 1 month (Steele et al.,

142    2001; http://psc.apl.washington.edu/nonwp_projects/PHC/Climatology.html). The sea

143    ice concentration (SIC) data were obtained from the NOAA/National Snow and Ice

144    Data Center Climate Data Record of Passive Microwave Sea Ice Concentration version

145  2, which has a resolution of 25 km × 25 km × 1 month (Meier et al., 2013;

146  http://nsidc.org/data/G02202). These data were averaged into 1° × 1° × 1 month

147  grid-cells. Zonal mean data for the atmospheric $CO_2$ mixing ratio ($xCO_{2a}$) were

148  retrieved from the NOAA Greenhouse Gas Marine Boundary Layer Reference data

149  product (Conway et al., 1994; http://www.esrl.noaa.gov/gmd/ccgg/mbl/index.html) and

150  were interpolated into 1° × 1° × 1 month grid-cells. We used monthly sea level pressure

151  data and the 6-hourly 10-m wind speeds from the U.S. National Centers for

152  Environmental Prediction–Department of Energy Reanalysis 2 (NCEP 2) (Kanamitsu et

153  al., 2002; http://www.esrl.noaa.gov/psd/data/gridded/data.ncep.reanalysis2.html). We

154  also used the 6-hourly 10-m wind speeds from the U.S. National Centers for

155  Atmospheric Prediction and the National Center for Atmospheric Research Reanalysis 1

156  (NCEP1) (Kalnay et al., 1996;

157  https://www.esrl.noaa.gov/psd/data/gridded/data.ncep.reanalysis.html) to optimize the

158  gas transfer velocity.

159   Surface nitrate measurements were extracted from GLODAPv2 (Key et al., 2015;

160  Olsen et al., 2016) and the World Ocean Database 2013 (Boyer et al., 2013).

161

162  **3. Methods**

163    3.1. Calculation of chlorophyll-a concentrations

164    We calculated Chl-a from Rrs by using the Arctic algorithm developed by Cota et al.

165    (2004). Several assessments have shown that the Arctic algorithm by Cota et al. (2004)

166    has a large uncertainty (e.g., Matsuoka et al., 2007; Lewis et al., 2016), so we evaluated

167    the sensitivity of our results to this choice by using two other algorithms for Chl-a: the

168    standard algorithm, of O'Reilly et al. (1998), and the coastal algorithm, of Tassan

169    (1994).

170       To ensure that we were working with Rrs relatively unaffected by suspended

171    sediments and colored dissolved organic matter, we masked the Chl-a data following the

172    method of Siswanto et al. (2013). We plotted the Rrs spectral slope between 412 and

173    555 nm ($Rrs_{555\text{-}412\ slope}$; $sr^{-1}\ nm^{-1}$) against logarithmically transformed Chl-a. We then

174    defined a boundary line separating phytoplankton-dominated grid-cells ($Rrs_{555\text{-}412\ slope} <$

175    boundary value) from potentially non-phytoplankton-dominated grid-cells ($Rrs_{555\text{-}412}$

176    $_{slope} \geq$ boundary value):

177

178       $Rrs_{555\text{-}412\ slope} = -0.000003\{\log(Chl\text{-}a)\}^2 + 0.00002\{\log(Chl\text{-}a)\} + 0.00006.$   (1)

179

180    Grid-cells were considered invalid and masked out if 1) $Rrs_{555\text{-}412\ slope} \geq$ boundary value,

181    and 2) Rrs at 555nm ($Rrs_{555}$) > 0.01 $sr^{-1}$ (or normalized water-leaving radiance > 2 mW

182    $cm^{-2}$ $\mu m^{-1}$ $sr^{-1}$; see Siswanto et al., 2011; Moore et al., 2012).

183       The criteria described in the previous paragraph could mask out grid-cells having

184    coccolithophore blooms, which are sometimes observed in the Arctic Ocean (e.g.,

185    Smyth et al., 2004), as they also have $Rrs_{555}$ > 0.01 $sr^{-1}$ (Moore et al., 2012). Unlike

186    waters dominated by non-phytoplankton particles, whose Rrs spectral shape peaks at

187    555 nm, the Rrs spectral shape of waters with coccolithophore blooms peaks at 490 or

188    510 nm (see Iida et al., 2002; Moore et al., 2012). Therefore, grid-cells with Rrs spectral

189    peaks at 490 or 510 nm (already classified using the criteria of Rrs at 490nm ($Rrs_{490}$) >

190    Rrs at 443nm ($Rrs_{443}$) and Rrs at 510nm ($Rrs_{510}$) > $Rrs_{555}$) were considered as

191    coccolithophore grid-cells, and were re-included.

192

193    3.2. Chlorophyll-a interpolation

194    Chl-a values calculated from Rrs are often missing because of cloud cover, low angle of

195    sunlight, or sea ice. For the period and area analyzed here, data are missing for 86 % of

196    the space and time grid-cells. Because $pCO_{2w}$ mapping requires a complete Chl-a field

197    without missing values, we interpolated Chl-a data as follows. 1) Chl-a was set to 0.01

198    mg $m^{-3}$ (minimum value of Chl-a) in high-latitude regions in winter when there was no

199    light (north of 80° N in December and January, and north of 88° N in November and

200    February). 2) Whenever SIC was greater than 99 %, Chl-a was set to 0.01 mg m$^{-3}$ (full

201    ice coverage, thus minimum Chl-a). We chose the strict criterion of SIC > 99 % because

202    weak but significant primary production has been found to occur under the sea ice in

203    regions with SIC around 90 % (Gosselin et al., 1997; Ulfsbo et al., 2014; Assmy et al.,

204    2017). 3) The remaining grid-cells with missing data were filled, wherever possible,

205    using Chl-a averaged over ±1° latitude and ±1° longitude; this mainly compensated for

206    missing Chl-a values as a result of cloud cover. 4) Parts of the remaining missing Chl-a

207    values, mainly for the pre-satellite period of January–August 1997, were set to the

208    monthly climatology Chl-a values based on the 18-year monthly mean from 1997 to

209    2014. 5) The final remaining missing Chl-a data, mainly for the marginal sea-ice zone,

210    were generated by linear interpolation using surrounding data. With each interpolation

211    step the number of the grid-cells with missing data decreased; 23 % of the grid-cells

212    without Chl-a data were filled by the first step, and in the same manner the subsequent

213    steps provided data for 12, 8, 5, and 52 %, respectively.

214

215    3.3. Gridding procedure for $p$CO$_2$ data

216    The individual $p$CO$_{2w}$ data were gridded to 1° × 1° × 1 month grid-cells covering the

217    years from 1997 to 2014 using the same procedure as Yasunaka et al. (2016). As

218    reference values, we calculated the long-term mean (i.e., the climatology) and its

219    standard deviation for a window size of ±5° of latitude, ±30° of longitude, and ±2

220    months (regardless of the year) for each 1° × 1° × 1 month grid-cell. We then eliminated

221    data in each grid-cell that differed by more than three standard deviations from the

222    climatology. We next recalculated the climatology and its standard deviation using a

223    smaller window size of ±2° of latitude, ±10° of longitude, and ±1 month (regardless of

224    the year) for each 1° × 1° × 1 month grid-cell. We again eliminated data that differed

225    from the climatology by more than three standard deviations.

226        This procedure identified in total about 0.5 % of the data as extreme or erroneous

227    values. These excluded values are randomly distributed in time and space. The

228    remaining observations were binned into 1° × 1° × 1 month grid-cells for each year

229    from 1997 to 2014. Although some studies have used $pCO_{2w}$ normalized to a certain

230    year, based on the assumption of a constant rate of increase for $pCO_{2w}$ (e.g., Takahashi

231    et al., 2009), we used "non-normalized" $pCO_{2w}$ values from all years; therefore, $pCO_{2w}$

232    can increase both non-linearly in time and non-uniformly in space. We believe that this

233    better represents the real variability and trends of $pCO_{2w}$.

234

235    3.4. $p$CO$_2$ estimation using a self-organizing map

236    We estimated $p$CO$_{2w}$ by the SOM technique used by Yasunaka et al. (2016), with the

237    exception that Chl-a was added as a parameter to train the SOM (a "training parameter")

238    in addition to SST, SSS, SIC, $x$CO$_{2a}$, and geographical position X (=sin[latitude] ×

239    cos[longitude]) and Y (=sin[latitude] × sin[longitude]). Chl-a, SST, SSS, and SIC are

240    closely related to processes causing variation in $p$CO$_{2w}$, such as primary production,

241    warming/cooling, mixing, and freshwater input, whereas $x$CO$_{2a}$ is related to seasonal

242    changes from terrestrial CO$_2$ uptake and release, and the anthropogenic CO$_2$ increase.

243    Thus, Chl-a, SST, SSS, and SIC represent spatio-temporal variability at seasonal to

244    interannual time-scales, and $x$CO$_{2a}$ acts as a temporal variable representing the seasonal

245    cycle and the long-term trend. The use of geographical position as a training parameter

246    can prevent a systematic spatial bias (Yasunaka et al., 2014).

247      Briefly, the SOM technique was implemented as follows: first, the approximately one

248    million 1° × 1° × 1 month grid-cells in the analysis region and period were assigned to

249    5000 groups, which are called "neurons", of the SOM by using the training parameters.

250    Second, each neuron was labeled, whenever possible, with the $p$CO$_{2w}$ value observed at

251    the grid-cell at which Chl-a, SST, SSS, SIC, $x$CO$_{2a}$, and X and Y values were most

252    similar to those of the neuron. Finally, each grid-cell in the analysis region and period

253    was assigned the $pCO_{2w}$ value of the neuron whose Chl-a, SST, SSS, SIC, $xCO_{2a}$, and X

254    and Y values were most similar to those at that grid-cell. If the most similar neuron was

255    not labeled with a $pCO_{2w}$ value, then the $pCO_{2w}$ value of the neuron that was most

256    similar *and* labeled was used. A detailed procedure can be found in Telzewski et al.

257    (2009) and Nakaoka et al. (2013).

258

259    3.5. Calculation of air–sea $CO_2$ fluxes

260    We calculated monthly air–sea $CO_2$ flux ($F$) values from the $pCO_{2w}$ values estimated in

261    Sect. 3.4 by using the bulk formula:

262

263        $$F = kL(pCO_{2w} - pCO_{2a}) ,$$                    (2)

264

265    where $k$ is the gas transfer velocity and $L$ is the solubility of $CO_2$. The solubility of $CO_2$

266    ($L$) was calculated as a function of SST and SSS (Weiss, 1974). We converted the

267    interpolated NOAA marine boundary layer $xCO_{2a}$ data (Sect. 2.2) to $pCO_{2a}$ by using

268    monthly sea-level pressure data and the water-vapor saturation pressure calculated from

269    monthly SST and SSS (Murray, 1967).

270        The gas transfer velocity $k$ was calculated by using the formula of Sweeney et al.

271    (2007):

272

273    $$k = 0.19\ (Sc/660)^{-0.5}\ \langle W_{NCEP2}{}^2 \rangle\,, \qquad\qquad (3)$$

274

275    where Sc is the Schmidt number of $CO_2$ in seawater at a given SST and was calculated

276    according to Wanninkhof (2014), "$\langle\ \rangle$" denotes the monthly mean, and $\langle W_{NCEP2}{}^2 \rangle$ is

277    the monthly mean of the second moment of the NCEP2 6-hourly wind speed. The

278    coefficient 0.19, which is the global average of $0.27\langle W_{NCEP1}{}^2 \rangle / \langle W_{NCEP2}{}^2 \rangle$, is based on

279    the one determined by Sweeney et al. (2007) but optimized for NCEP2 winds following

280    the same method as Schuster et al. (2013) and Wanninkhof et al. (2013).

281        The suppression of gas exchange by sea ice was accounted for by correcting the air–

282    sea $CO_2$ fluxes using the parameterization presented by Loose et al. (2009); the flux is

283    proportional to $(1\text{-}SIC)^{0.4}$. The SIC effect used in this study is consistent with the linear

284    SIC effect derived from another approach by Takahashi et al. (2009) and Butterworth

285    and Miller (2016) within the uncertainty of 30%. Following Bates et al. (2006), in the

286    regions with SIC > 99 %, we used SIC = 99 % to allow for non-negligible rates of air–

287    sea $CO_2$ exchange through leads, fractures, and brine channels (Semiletov et al., 2004;

288    Fransson et al., 2017).

289

290  **4. Uncertainty**

291  4.1. Uncertainty in chlorophyll-a concentration data

292  Figure 3 shows original and interpolated Chl-a for 2012 as an example. Most

293  interpolated Chl-a data are low concentrations because of high SIC and lack of daylight.

294  Overall, the interpolated Chl-a data seem to fit well with the original data.

295      To evaluate our choice of Chl-a algorithm (i.e. the Arctic algorithm of Cota et al.,

296  2004), we compared its calculated Chl-a values with those determined by using the

297  standard algorithm of O'Reilly et al. (1998) and the coastal algorithm of Tassan (1994).

298  The root mean square difference (RMSD) and correlation coefficient ($r$) between the

299  original (i.e. non-interpolated) Chl-a values determined with the Arctic algorithm and

300  the standard algorithm are 0.80 mg m$^{-3}$ and 0.90, respectively, and between those

301  determined with the Arctic algorithm and the coastal algorithm are 0.81 mg m$^{-3}$ and

302  0.87, respectively (Table 1). For the interpolated Chl-a values, they are 0.37 mg m$^{-3}$ and

303  0.92, and 0.48 mg m$^{-3}$ and 0.86, respectively. The lower RMSD results from the fact

304  that most of the interpolated Chl-a values represent low concentrations. The $p\mathrm{CO}_{2w}$ and

305  $CO_2$ fluxes determined using Chl-a from any of these algorithms as input to the SOM

306  are consistent within uncertainties of the $p\mathrm{CO}_{2w}$ and $CO_2$ flux estimates (see Sects. 4.2

307     and 4.3 below).

308         To validate our Chl-a interpolation, we repeated the interpolation after randomly

309     eliminating 10 % of the satellite Chl-a values. We then used the eliminated original

310     Chl-a data as independent data for validation. The RMSD and correlation coefficient

311     between the interpolated and the independent original Chl-a data are 0.90 mg m$^{-3}$ and

312     0.80, respectively. It means the interpolated Chl-a generally reproduced the Chl-a

313     concentrations, and therefore is a meaningful parameter in the SOM process.

314

315     4.2. Uncertainty of $p$CO$_{2w}$ mapping

316     Both observed and estimated $p$CO$_{2w}$ tended to be high in the subpolar North Atlantic,

317     the Laptev Sea, and the Canada Basin, and low in the Greenland Sea and the Barents

318     Sea (Figs. 4a and 4b; Note that the spatial change depicted in Figs. 4a and 4b include

319     differences in the observed seasons depending on the regions). However, the east–west

320     contrast in the Bering Sea and the contrast between the Canada Basin and the Chukchi

321     Sea are weaker in our estimates than those in the observations, and mean bias and

322     RMSD are relatively large in those areas (Figs. 5a and 5b). The temporal changes in the

323     observed and estimated $p$CO$_{2w}$ are in phase, although the variability of the estimated

324     values is somewhat suppressed compared to that of the observed data (Fig. 4c; Note that

325 the temporal change depicted in Fig. 4c includes changes in the positions of the

326 observation points). Mean bias and RMSD show no long-term change (Fig. 5c).

327 The correlation coefficient between estimated and observed $pCO_{2w}$ values is 0.82,

328 and the RMSD is 30 µatm, which is 9 % of the average and 58 % of the standard

329 deviation of the observed $pCO_{2w}$ values (a performance level of 58 % is categorized as

330 "good" by Maréchal [2004]). The differences between the estimated and observed

331 values stem not only from the estimation error but also from the error of the gridded

332 observation data. The uncertainty of the $pCO_{2w}$ measurements is 2–5 µatm (Bakker et

333 al., 2014), the uncertainty of the $pCO_{2w}$ values calculated from dissolved inorganic

334 carbon and total alkalinity can be up to 14 µatm (Lueker et al., 2000), and the sampling

335 error of the gridded $pCO_{2w}$ observation data was deduced from the standard errors of

336 monthly observed $pCO_{2w}$ in the $1° \times 1°$ grid-cells to be 7 µatm (Yasunaka et al., 2016).

337 To validate our estimated $pCO_{2w}$ values for periods and regions without any observed

338 data, we repeated the mapping experiments after systematically excluding some of the

339 observed $pCO_{2w}$ data when labeling the neurons; four experiments were carried out, by

340 excluding data (1) for 1997–2004, (2) for January to April, (3) from north of 80°N, and

341 (4) from the Laptev Sea (90°E – 150°E), where there are only a few $pCO_{2w}$ observations.

342 The RMSDs between the estimates and the excluded observations are 54 µatm on

343 average, which is 1.8 times the RMSDs of the estimates based on all observations.

344 Hence the uncertainty in $pCO_{2w}$ might be as large as 16 % in regions and periods

345 without data.

346

347 4.3. Uncertainty of $CO_2$ flux estimates

348 Signorini and McClain (2009) estimated the uncertainty of the $CO_2$ flux resulting from

349 uncertainties in the gas exchange parameterization to be 36 %, and that resulting from

350 uncertainties in the wind data to be 11 %. The uncertainty for SIC is 5 % (Cavalieri et

351 al., 1984; Gloersen et al., 1993; Peng et al., 2013). The standard error of the sea-ice

352 effect on gas exchange was estimated to about 30 % by Loose et al. (2009). The

353 uncertainty of $pCO_{2a}$ is about 0.5 µatm

354 (http://www.esrl.noaa.gov/gmd/ccgg/mbl/mbl.html), and that of $pCO_{2w}$ was 30 µatm

355 (Sect. 4.2); therefore, we estimated the uncertainty of $\Delta pCO_2$ ($=pCO_{2w} - pCO_{2a}$) to be

356 34 % (average $\Delta pCO_2$ in the analysis domain and period was −89 µatm). The overall

357 uncertainty of the estimated $CO_2$ fluxes is 59 % ($[0.36^2 + 0.11^2 + 0.05^2 + 0.3^2 +$

358 $0.34^2]^{1/2}$) in the sea-ice covered region and 51 % ($[0.36^2 + 0.11^2 + 0.05^2 + 0.34^2]^{1/2}$) in

359 the ice-free region. In regions and periods without any observed data, where the

360 uncertainty in $pCO_{2w}$ is 54 µatm and the uncertainty of the $\Delta pCO_2$ estimates can be as

361   high as 61 %, the uncertainty is 78 % ($[0.36^2 + 0.11^2 + 0.05^2 + 0.3^2 + 0.61^2]^{1/2}$) in

362   sea-ice covered regions, and 72 % ($[0.36^2 + 0.11^2 + 0.05^2 + 0.61^2]^{1/2}$) in ice-free regions.

363   The average of the estimated $CO_2$ flux in the analysis domain and period is 4.8 mmol

364   $m^{-2}\,d^{-1}$; hence the uncertainty of the $CO_2$ flux estimate corresponds to 2.8 mmol $m^{-2}\,d^{-1}$

365   in sea-ice covered regions and 2.4 mmol $m^{-2}\,d^{-1}$ in ice-free regions. In regions and

366   periods without observed data, the uncertainty corresponds to 3.7 mmol $m^{-2}\,d^{-1}$ in the

367   sea-ice covered region and 3.5 mmol $m^{-2}\,d^{-1}$ in ice-free regions.

368

369   **5. Results and discussion**

370   5.1. Relationship between $p$CO$_2$ and chlorophyll-a

371   We compared the observed $p$CO$_{2w}$ and the original non-interpolated Chl-a in spring

372   (March–May) and summer (July–September) (Fig. 6a and b). In spring, when much of

373   the Arctic Ocean is ice-covered, Chl-a is high in the Barents Sea and the Bering Strait

374   (>1 mg $m^{-3}$). In summer, when the ice cover is less extensive, Chl-a is high in the

375   Chukchi Sea, the Kara Sea, the Laptev Sea, and the East Siberian Sea (>1 mg $m^{-3}$) and

376   especially high in the coastal region (>2 mg $m^{-3}$). $p$CO$_{2w}$ is high in the Norwegian Sea

377   in spring; and also high in the Kara Sea, the Laptev Sea and the Canada Basin during

378   summer (>300 µatm). On the other hand, it is lower in the Chukchi Sea, Bering Strait

379     area and the sea-ice edge region of the Eurasian Basin in summer (<300 µatm). The

380     overall relationship between $p\mathrm{CO}_{2w}$ and Chl-a is negative where Chl-a $\leq 1$ mg m$^{-3}$ (70%

381     of all the data; correlation coefficient $r = -0.36$, $P < 0.01$), but there is no significant

382     relationship where Chl-a $> 1$ mg m$^{-3}$ (Fig. 7), as also shown by Olsen et al. (2008) in the

383     subpolar North Atlantic. That is probably because high Chl-a usually appeared in the

384     coastal region (Fig. 6b) which are affected by the river runoff.

385      To determine the spatial variability of the relationship between $p\mathrm{CO}_{2w}$ and Chl-a, we

386     calculated the correlation coefficients between $p\mathrm{CO}_{2w}$ and Chl-a in a window of ±5° of

387     latitude, and ±30° of longitude for each monthly 1° × 1° grid-cell (Fig. 6d). We found

388     negative relationships between $p\mathrm{CO}_{2w}$ and Chl-a in the Greenland/Norwegian Seas and

389     the Canada Basin. In the Greenland/Norwegian Seas, the relationship between $p\mathrm{CO}_{2w}$

390     and Chl-a is strongly negative (r < –0.4) in spring and weakly negative (–0.4 < r < 0) in

391     summer. Chl-a there is higher in summer than in spring, whereas nutrient concentrations

392     are high in spring and low in summer (Fig. 6c). These correlations suggest that primary

393     production draws down the $p\mathrm{CO}_{2w}$ in spring, whereas in summer the primary production

394     mostly depends on regenerated nutrients (Harrison and Cota, 1991) and the net $\mathrm{CO}_2$

395     consumption is small, as also reported for the subpolar North Atlantic (Olsen et al.,

396     2008). In the eastern Barents Sea, the Kara Sea and the East Siberian Sea, and the

397    Bering Strait, the relationships are positive because of water with high $pCO_{2w}$ and Chl-a

398    in the coastal region subjected to river discharge (Murata, 2006; Semiletov et al., 2007;

399    Anderson et al., 2009; Manizza et al., 2011). In the Chukchi Sea, the relationship is

400    weak ($-0.2 < r < 0.2$), probably because the relationship is on smaller spatial and

401    temporal scales than those represented by the window size used here, as shown by

402    Mucci et al. (2010). Calcifying plankton bloom would also weaken the correlation since

403    it will affect the $pCO_{2w}$ in the different way (Shutler et al., 2013; Fransson et al., 2017).

404

405    5.2. Spatiotemporal $CO_2$ flux variability

406       The 18-year annual mean $CO_2$ flux distribution shows that all areas of the Arctic

407    Ocean and its adjacent seas were net $CO_2$ sinks over the time period that we

408    investigated (Fig. 8). The annual $CO_2$ influx to the ocean is strong in the

409    Greenland/Norwegian Seas ($9 \pm 3$ mmol m$^{-2}$ d$^{-1}$; 18-year annual mean $\pm$ uncertainty

410    averaged over the area shown in Fig. 1), the Barents Sea ($10 \pm 3$ mmol m$^{-2}$ d$^{-1}$), and the

411    Chukchi Sea ($5 \pm 3$ mmol m$^{-2}$ d$^{-1}$). In contrast, influx is weak and not statistically

412    significantly different from zero in the Eurasian Basin and the Canada Basin, or in the

413    Laptev Sea and the East Siberian Sea. Our annual $CO_2$ flux estimates are consistent with

414    those reported by Yasunaka et al. (2016) and other previous studies (Bates and Mathis,

415    2009, and references therein). The estimated 18-year average $CO_2$ influx to the Arctic

416    Ocean is $5 \pm 3$ mmol m$^{-2}$ d$^{-1}$, equivalent to an uptake of $180 \pm 130$ TgC y$^{-1}$ for the

417    ocean area north of 65° N, excluding the Greenland/Norwegian Seas and Baffin Bay

418    ($10.7 \times 10^6$ km$^2$; see Fig. 1). This is within the range of other estimates (81–199 TgC y$^-$

419    $^1$; Bates and Mathis, 2009).

420    The $CO_2$ influxes to the Greenland/Norwegian Seas, the Barents Sea, and the

421    Chukchi Sea are strongest in October (>10 mmol m$^{-2}$ d$^{-1}$; Fig. 9), when the winds

422    strengthen with the approach of winter and the SIC and $pCO_{2w}$ are still as low as in the

423    summer. The total $CO_2$ influx to the Arctic Ocean is also strongest in October. The $CO_2$

424    influx shows a secondary maximum in February in the Greenland/Norwegian Seas and

425    the Barents Sea because the strongest winds occur in that month (not shown).

426    The $CO_2$ influx has been increasing in the Greenland Sea and northern Barents Sea,

427    and decreasing in the Chukchi Sea and southern Barents Sea (Fig. 10). The $CO_2$ flux

428    trend corresponds well with the $\Delta pCO_2$ trend, which in turn corresponds well with the

429    SST trend. High $pCO_{2w}$ (>500 µatm) has been sometimes observed in the Chukchi Sea

430    after 2010 (Hauri et al. 2013). The increasing $CO_2$ influx in the northern Barents Sea

431    also corresponds with the sea-ice retreat.

432

### 5.3. Impact of incorporating chlorophyll-a data in the SOM

To determine the impact of including Chl-a data in the SOM process, the analyses were

repeated without Chl-a data. The RMSD of the resulting estimated $pCO_{2w}$ values is 33

µatm, 3 µatm larger than the uncertainty of the estimates generated by including Chl-a

in the SOM. Chl-a data thus improved the $pCO_{2w}$ estimate (namely, a 10 % reduction of

RMSD), even though 40 % of the Chl-a data labeled with $pCO_{2w}$ observations were

interpolated Chl-a values. This improvement resulted mainly from an improved

representation of the seasonal cycle of $pCO_{2w}$ by the SOM technique, which reproduced

the observed cycle better when Chl-a was included (upper panels of Fig. 11).

The seasonal cycles of $pCO_{2w}$ estimates derived with the inclusion of Chl-a has a

larger amplitude than the uncertainties, whereas the uncertainties are larger than the

seasonal amplitude of $pCO_{2w}$ derived without Chl-a (lower panels of Fig. 11). Note that

the much larger seasonal amplitude in observed $pCO_{2w}$ in each region (upper panels of

Fig. 11) is due to the seasonal changes in the extent of the observed area: area average

of observed $pCO_{2w}$ in winter was obtained mostly from the data in the lower latitudes,

where $pCO_{2w}$ tends to be higher than that in the higher latitudes. The winter $CO_2$ influx

in the Greenland/Norwegian Seas estimated including Chl-a is about 3 mmol $m^{-2}$ $d^{-1}$

less than those calculated without using Chl-a (Fig. 9), but this difference is smaller than

451   the uncertainties. The pattern in trends is similar to that for the estimates without using

452   Chl-a (see Fig. 10 in Yasunaka et al., 2016).

453      The inclusion of Chl-a data also reduced the uncertainty of the estimated annual

454   air-sea $CO_2$ flux integrated over the entire Arctic Ocean. Compared to the flux estimate

455   determined by Yasunaka et al. (2016) of $180 \pm 210$ TgC y$^{-1}$, the $CO_2$ uptake in the

456   Arctic Ocean estimated here is significant within its uncertainty ($180 \pm 130$ TgC y$^{-1}$).

457   This improvement is the result of 1) the inclusion of Chl-a data in the SOM process

458   (which reduced the uncertainty by 23 %); 2) the separate uncertainty estimates for

459   ice-free and ice-covered regions (8 %); and 3) the addition of new observational $pCO_{2w}$

460   data (7 %).

461

462   **6. Conclusions**

463   By applying an SOM technique with the inclusion of Chl-a data to estimate $pCO_{2w}$, we

464   produced monthly maps of air–sea $CO_2$ fluxes from 1997 to 2014 for the Arctic Ocean

465   and its adjacent seas north of 60° N. The overall relationship between $pCO_{2w}$ and Chl-a

466   is negative, consistent with it being determined by primary production, but the

467   relationship depended on the season and the region. Adding Chl-a to the SOM process

468   improved representation of the seasonal cycle of $pCO_{2w}$. A major goal of the

469   carbon-cycle research community in recent years has been to reduce the uncertainty in

470   estimates of carbon reservoirs and fluxes. Our results contribute to this in that $CO_2$

471   uptake in the Arctic Ocean is demonstrated with high significance. The resulting

472   estimate of the annual Arctic Ocean $CO_2$ uptake of 180 TgC $y^{-1}$ is significant with an

473   uncertainty of only $\pm$ 130 TgC $y^{-1}$. This is a substantial improvement over earlier

474   estimates, and is due mainly to the incorporation of Chl-a data.

475      The addition of new observational data from SOCATv4 and GLODAPv2 reduced the

476   overall uncertainty in the mapped $pCO_{2w}$: a 33 % increase in the number of observations

477   induced a 7 % reduction in the uncertainty. However, there are still too few observations

478   in the Kara Sea, the Laptev Sea, the East Siberian Sea and the Eurasian Basin to

479   determine seasonal and interannual variations there. To improve our understanding of

480   the variability in air–sea $CO_2$ fluxes in the Arctic, it is of critical importance to obtain

481   additional ocean $CO_2$ measurements to fill these data gaps.

482      The monthly $CO_2$ flux data presented in this paper will be available at the JAMSTEC

483   website (http://www.jamstec.go.jp/res/ress/yasunaka/co2flux_v2).

484

485   **Acknowledgments**

486    We thank the many researchers and funding agencies responsible for the collection of

487    data and quality control for their contributions to SOCAT and GLODAPv2. We are

488    grateful for the use of the CO2SYS program obtained from the Carbon Dioxide

489    Information Analysis Center (http://cdiac.ornl.gov/oceans/co2rprt.html), and SOM

490    Toolbox Version 2 developed by the Laboratory of Information and Computer Science

491    at Helsinki University of Technology (http://www.cis.hut.fi/projects/somtoolbox). We

492    thank ACRI-ST, France, for developing, validating, and distributing the GlobColour

493    data used in this work. This work was financially supported by the Arctic Challenge for

494    Sustainability (ArCS) Project funded by the Ministry of Education, Culture, Sports,

495    Science and Technology, Japan. Are Olsen was supported by grants from the Norwegian

496    Research Council (Subpolar North Atlantic Climate States [SNACS] 229752 and the

497    Norwegian component of the Integrated Carbon Observation System [ICOS-Norway]

498    245927). Mario Hoppema was partly supported by the German Federal Ministry of

499    Education and Research (grant no. 01LK1224I; ICOS-D). Siv K. Lauvset acknowledges

500    support from the Norwegian Research Council (VENTILATE, 229791) and the EU

501    H2020 project AtlantOS (grant agreement no. 633211). Rik Wanninkhof and Taro

502    Takahashi acknowledge support from the Office of Oceanic and Atmospheric Research

503    (OAR) of the United States NOAA, including resources from the Ocean Observation

504    and Monitoring Division of the Climate Program Office (fund reference100007298).

505

506    **References**

507    Anderson, L. G., Jutterström, S., Hjalmarsson, S., Wåhlström, I., and Semiletov, I. P.:

508        Out-gassing of $CO_2$ from Siberian Shelf seas by terrestrial organic matter

509        decomposition, Geophys. Res. Lett., 36, L20601, doi:10.1029/2009GL040046, 2009.

510    Ardyna, M., Babin, M., Gosselin, M., Devred, E., Rainville, L., and Tremblay, J.-É.:

511        Recent Arctic Ocean sea ice loss triggers novel fall phytoplankton blooms, Geophys.

512        Res. Lett., 41, 6207–6212, doi:10.1002/2014GL061047, 2014.

513    Arrigo, K. R., and van Dijken, G. L.: Annual cycles of sea ice and phytoplankton near

514        Cape Bathurst, southeastern Beaufort Sea, Canadian Arctic, Geophys. Res. Lett., 31,

515        L08304, doi:10.1029/2003GL018978, 2004.

516    Assmy P. M. Fernandez-Mendez, Duarte, P., Meyer, A., Randelhoff, A., Mundy, C. J.,

517        Olsen, L. M., Kauko, H. M., Bailey, A., Chierici, M., Cohen, L., Doulgeris, A. P.,

518        Ehn, J. K., Fransson, A., Gerland, S., Hop, H., Hudson, S. R., Hughes, N., Itkin, P. ,

519        Johnsen, G. , King, J. A., Koch, B. P. , Koenig, Z., Kwasniewski, S., Laney, S. R.,

520        Nicolaus, M., Pavlov, A. K., Polashenski, C. M., Provost, C., Rösel, A., Sandbu, M.,

521        Spreen, G., Smedsrud, L. H., Sundfjord, A., Taskjelle, T., Tatarek, A., Wiktor, J.,

522    Wagner, P. M., Wold, A., Steen, H., and Granskog, M. A.: Leads in Arctic pack ice

523    enable early phytoplankton blooms below snow-covered sea ice. Scientific Report,

524    7:40850, DOI: 10.1038/srep40850, 2017.

525  Bakker, D. C. E., Pfeil, B., Smith, K., Hankin, Olsen, A., Alin, C. Cosca, S. R.,

526    Harasawa, S., Kozyr, A., Nojiri, Y., O'Brien, K. M., Schuster, U., Telszewski, M.,

527    Tilbrook, B., Wada, C., Akl, J., Barbero, L., Bates, N., Boutin, J., Cai, W.-J., Castle,

528    R. D., Chavez, F. P., Chen, L., Chierici, M., Currie, K., de Baar, H. J. W., Evans, W.,

529    Feely, R. A., Fransson, A., Gao, Z., Hales, B., Hardman-Mountford, N., Hoppema,

530    M., Huang, W.-J., Hunt, C. W., Huss, B., Ichikawa, T., Johannessen, T., Jones, E. M.,

531    Jones, S., Jutterstrøm, S., Kitidis, V., Körtzinger, A., Lauvset, S. K., Lefèvre, N.,

532    Manke, A. B., Mathis, J. T., Merlivat, L., Metzl, N., Murata, A., Newberger, T., Ono,

533    T., Park, G.-H., Paterson, K., Pierrot, D., Ríos, A. F., Sabine, C. L., Saito, S.,

534    Salisbury, J., Sarma, V. V. S. S., Schlitzer, R., Sieger, R., Skjelvan, I., Steinhoff, T.,

535    Sullivan, K., Sun, H., Sutton, A. J., Suzuki, T., Sweeney, C., Takahashi, T., Tjiputra,

536    J., Tsurushima, N., van Heuven, S. M. A. C., Vandemark, D., Vlahos, P., Wallace, D.

537    W. R., Wanninkhof, R., and Watson, A. J.: An update to the Surface Ocean $CO_2$ atlas

538    (SOCAT version 2). Earth System Science Data, 6, 69–90,

539    doi:10.5194/essd-6-69-2014, 2014.

540    Bakker, D. C. E., Pfeil, B., Smith, K., Harasawa, S., Landa, C., Nakaoka, S., Nojiri, Y.,

541    Metzl, N., O'Brien, K. M., Olsen, A., Schuster, U., Tilbrook, B., Wanninkhof, R.,

542    Alin, S. R., Barbero, L., Bates, N. R., Bianchi, A. A., Bonou, F., Boutin, J., Bozec, Y.,

543    Burger, E., Cai, W.-J., Castle, R. D., Chen, L., Chierici, M., Cosca, C., Currie, K.,

544    Evans, W., Featherstone, C., Feely, R. A., Fransson, A., Greenwood, N., Gregor, L.,

545    Hankin, S., Hardman-Mountford, N. J., Harlay, J., Hauck, J., Hoppema, M., Humpt,

546    L., Monteiro, P., Munro, D., Murata, A., Newberger, T., Omar, A. M., Ono, T.,

547    Paterson, K., Pierrot, D., Robbins, L. L., Sabine, C. L., Saito, S., Salisbury, J.,

548    Schneider, B., Schlitzer, R., Sieger, R., Skjelvan, I., Steinhoff, T., Sullivan, K. F., St,

549    L., Monteiro, P., Munro, D., Murata, A., Newberger, T., Omar, A. M., Ono, T.,

550    Paterson, K., Pierrot, D., Robbins, L. L., Sabine, C. L., Saito, S., Salisbury, J.,

551    Schneider, B., Schlitzer, R., Sieger, R., Skjelvan, I., Steinhoff, T., Sullivan, K. F.,

552    Sutherland, S. C., Sutton, A. J., Sweeney, C., Tadokoro, K., Takahashi, T., Telszewski,

553    M., Van Heuven, S. M. A. C., Vandemark, D., Wada, C., Ward, B., and Watson, A. J.:

554    A multi-decade record of high quality $fCO_2$ data in version 3 of the Surface Ocean

555    $CO_2$ Atlas (SOCAT). Earth System Science Data, 8, 383–413.

556    doi:10.5194/essd-8-383-2016, 2016.

557    Bates, N. R., and Mathis, J. T.: The Arctic Ocean marine carbon cycle: evaluation of

558    air-sea $CO_2$ exchanges, ocean acidification impacts and potential feedbacks,

559    Biogeosciences, 6, 2433-2459, doi:10.5194/bg-6-2433-2009, 2009.

560    Bates, N. R., Moran, S. B., Hansell, D. A., and Mathis, J. T.: An increasing $CO_2$ sink in

561    the Arctic Ocean due to sea-ice loss, Geophys. Res. Lett., 33, L23609,

562    doi:10.1029/2006GL027028, 2006.

563    Bates, N. R., Garley, R., Frey, K. E., Shake, K. L., and Mathis J. T.: Sea-ice melt

564    $CO_2$-carbonate chemistry in the western Arctic Ocean: meltwater contributions to

565    air-sea $CO_2$ gas exchange, mixed layer properties and rates of net community

566    production under sea ice. Biogeosciences, 11, 6769–6789,

567    doi:10.5194/bg-11-6769-2014., 2014

568    Boyer, T. P., Antonov, J. I., Baranova, O. K., Coleman, C., Garcia, H. E., Grodsky, A.,

569    Johnson, D. R., Locarnini, R. A., Mishonov, A. V., O'Brien, T. D., Paver, C. R.,

570    Reagan, J. R., Seidov, D., Smolyar, I. V., and Zweng, M. M.: World Ocean Database

571    2013. Sydney Levitus, Ed.; Alexey Mishonov, Technical Ed.; NOAA Atlas NESDIS

572    72, 209 pp, 2013.

573    Butterworth, B. J., and Miller, S. D.: Air-sea exchange of carbon dioxide in the Southern

574    Ocean and Antarctic marginal ice zone. Geophys. Res. Lett., 43, 7223–7230,

575    doi:10.1002/2016GL069581, 2016.

576    Cai, W.J., Chen, L. Q., Chen, B. S., Gao, Z. Y., Lee, S. H., Chen, J. F., Pierrot, D.,

577    Sullivan, K., Wang, Y.C., Hu, X. P., Huang, W. J., Zhang, Y. H., Xu, S. Q., Murata, A.,

578    Grebmeier, J. M., Jones, E. P., and Zhang, H. S.: Decrease in the $CO_2$ uptake capacity

579    in an ice-free Arctic Ocean Basin. Science, 329, 556–559,

580    doi:10.1126/science.1189338, 2010.

581    Cavalieri, D. J., Gloersen, P., and Campbell, W. J.: Determination of sea ice parameters

582    with the NIMBUS-7 SMMR, J. Geophys. Res., 89, 5355–5369, 1984.

583    Chierici, M., Olsen, A., Johannessen, T., Trinañes, J., Wanninkhof, R.: Algorithms to

584    estimate $CO_2$ in the northern North Atlantic using observations, satellite and ocean

585    analysis data, Deep Sea Research II, 56, 630–639, doi:10.1016/j.dsr2.2008.12.01,

586    2009.

587    Chierici, M, Fransson, A., Lansard, B., Miller, L. A., Mucci, A., Shadwick, E., Thomas,

588    H., Tremblay, J.-E., and Papakyriakou, T.: The impact of biogeochemical processes

589    and environmental factors on the calcium carbonate saturation state in the

590    Circumpolar Flaw Lead in the Amundsen Gulf, Arctic Ocean. J. Geophys. Res., 116,

591    C00G09, doi:10.1029/2011JC007184, 2011.

592    Conway, T.J., Tans, P. P., Waterman, L. S., Thoning, K. W., Kitzis, D. R., Masarie, K. A.,

593    and Zhang, N.: Evidence for interannual variability of the carbon cycle from the

594    NOAA/CMDL global air sampling network. J. Geophys. Res., 99, 22831–22855,

595    1994.

596  Cota, G. F., Wang, J., and Comiso, J. C.: Transformation of global satellite chlorophyll

597    retrievals with a regionally tuned algorithm, Remote Sens. Environ. 89, 326–350,

598    doi:10.1016/j.rse.2004.01.005, 2004.

599  Dickson, A. G.: Standard potential of the reaction: AgCl(s) + 1/2H$_2$(g) = Ag(s) +

600    HCl(aq), and the standard acidity constant of the ion HSO$_4^-$ in synthetic seawater

601    from 273.15 to 318.15 K. J. Chemical Thermodynamics, 22, 113–127, 1990.

602  Else, B. G. T., Galley, R. J., Lansard, B., Barber, D. G., Brown, K., Miller, L. A., Mucci,

603    A., Papakyriakou, T. N., Tremblay, J.-É., and Rysgaard, S.: Further observations of a

604    decreasing atmospheric CO$_2$ uptake capacity in the Canada Basin (Arctic Ocean) due

605    to sea ice loss, Geophys. Res. Lett., 40, 1132–1137, doi:10.1002/grl.50268, 2013.

606  Fransson, A., Chierici, M., Skjelvan, I., Olsen, A., Assmy, P., Peterson, A. K., Spreen, G.,

607    and Ward, B.: Effects of sea-ice and biogeochemical processes and storms on

608    under-ice water $f$CO$_2$ during the winter-spring transition in the high Arctic Ocean:

609    Implications for sea-air CO$_2$ fluxes. J. Geophys. Res., doi:10.1002/2016JC012478,

610    2017.

611  Gao, Z., Chen, L., Sun, H., Chen, B., and Cai, W.-J.: Distributions and air–sea fluxes of

612    carbon dioxide in the Western Arctic Ocean, Deep-Sea Res. II, 81–84, 46–52,

613    doi:10.1016/j.dsr2.2012.08.021, 2012.

614    Gloersen, P., Campbell, W. J., Cavalieri, D. J., Comiso, J. C., Parkinson, C. L., and

615    Zwally, H. J.: Arctic and Antarctic sea ice, 1978–1987: Satellite passive-microwave

616    observations and analysis, NASA Spec. Publ., 511, 290 pp, 1993.

617    Gosselin, M., Levasseur, M., Wheeler, P. A., Horner, R. A., and B. C. Booth: New

618    measurements of phytoplankton and ice algal production in the Arctic Ocean,

619    Deep-Sea Res. II, 44, 1623–1644, doi:10.1016/S0967-0645(97)00054-4, 1997.

620    Harrison, W. G., and Cota., G. F.: Primary production in polar waters: relation to

621    nutrient availability, Polar Research, 10, 87–104,

622    doi:10.1111/j.1751-8369.1991.tb00637.x, 1991.

623    Hauri, C., Winsor, P., Juranek, L. W., McDonell, A. M. P., Takahashi, T. and Mathis, J.

624    T.: Wind-driven mixing causes a reduction in the strength of the continental shelf

625    carbon pump in the Chukchi Sea, Geophys. Res. Letters, 40, 5932-5936,

626    doi:10.1002/2013GL058267, 2013.

627    Iida, T., Saitoh, S. I., Miyamura, T., Toratani, M., Fukushima, H., and Shiga, N.:

628    Temporal and spatial variability of coccolithophore blooms in the eastern Bering Sea,

629    1998-2001, Prog. Oceanogr., 55, 165–175, 2002.

630    Kalnay, E., Kanamitsu, M., Kistler, R., Collins, W., Deaven, D., Gandin, L., Iredell, M.,

631       Saha, S., White, G., Woollen, J., Zhu, Y., Chelliah, M., Ebisuzaki, W., Higgins, W.,

632       Janowiak, J., Mo, K. C., Ropelewski, C., Wang, J., Leetmaa, A., Reynolds, R., Jenne,

633       R., and Joseph, D., The NCEP/NCAR 40-Year Reanalysis Project". Bull. Amer.

634       Meteor. Soc., 77, 437–471, 1996.

635    Kanamitsu, M., Ebisuzaki, W., Woollen, J., Yang, S-K, Hnilo, J. J., Fiorino, M., and

636       Potter, G. L., NCEP-DOE AMIP-II Reanalysis (R-2), Bull. Amer. Meteor. Soc., 83,

637       1631–1643, 2002.

638    Key, R.M., Olsen, A., van Heuven, S., Lauvset, S. K., Velo, A., Lin, X., Schirnick, C.,

639       Kozyr, A., Tanhua, T., Hoppema, M., Jutterström, S., Steinfeldt, R., Jeansson, E.,

640       Ishii, M., Perez, F. F., and T. Suzuki: Global Ocean Data Analysis Project, Version 2

641       (GLODAPv2), ORNL/CDIAC-162, ND-P093. Carbon Dioxide Information Analysis

642       Center, Oak Ridge National Laboratory, US Department of Energy, Oak Ridge,

643       Tennessee. doi: 10.3334/CDIAC/OTG.NDP093_GLODAPv2, 2015.

644    Lefèvre, N., Watson, A. J., and Watson, A. R.: A comparison of multiple regression and

645       neural network techniques for mapping in situ $pCO_2$ data, Tellus B, 57: 375–384.

646       doi:10.1111/j.1600-0889.2005.00164.x, 2005.

647    Lewis, E., and Wallace, D. W. R.: Program Developed for $CO_2$ System Calculations.

648    ORNL/CDIAC-105. Carbon Dioxide Information Analysis Center, Oak Ridge

649    National Laboratory, U.S. Department of Energy, Oak Ridge, Tennessee, 1998.

650    Lewis, K.M., Mitchell, B.G., van Dijken, G.L., and Arrigo, K.R.: Regional chlorophyll

651    a algorithms in the Arctic Ocean and their effect on satellite-derived primary

652    production estimates, Deep Sea Research-II, 130, 17–24,

653    doi:10.1016/j.dsr2.2016.04.020, 2016.

654    Loose, B., McGillis, W. R., Schlosser, P., Perovich, D., and Takahashi, T.: Effects of

655    freezing, growth, and ice cover on gas transport processes in laboratory seawater

656    experiments, Geophys. Res. Lett., 36, L05603, doi:10.1029/2008GL036318, 2009.

657    Lueker, T. J., Dickson, A. G., and Keeling, C. D.: Ocean $pCO_2$ calculated from

658    dissolved inorganic carbon, alkalinity, and equations for K1 and K2: validation based

659    on laboratory measurements of $CO_2$ in gas and seawater at equilibrium, Mar. Chem.,

660    70, 105–119, 2000.

661    Manizza, M., Follows, M. J., Dutkiewicz, S., Menemenlis, D., McClelland, J. W., Hill,

662    C. N., Peterson, B. J., and R. M. Key: A model of the Arctic Ocean carbon cycle, J.

663    Geophys. Res., 116, C12020, doi:10.1029/2011JC006998, 2011.

664    Maréchal, D., A soil-based approach to rainfall-runoff modelling in ungauged

665    catchments for England and Wales. PhD thesis, Cranfield University. 157 pp, 2004.

666 Maritorena, S., d'Andon, O. H. F., Mangin, A., and Siegel, D. A.: Merged satellite ocean

667 color data products using a bio-optical model: Characteristics, benefits and issues,

668 Remote Sensing of Environment, 114, 1791-1804, doi:10.1016/j.rse.2010.04.002,

669 2010.

670 Matsuoka, A., Huot, Y., Shimada, K., Saitoh, S., and Babin, M.: Bio-optical

671 characteristics of the western Arctic Ocean: Implications for ocean color algorithms,

672 Can. J. Remote Sens., 33, 503–518, doi:10.5589/m07-059, 2007.

673 Meier, W., Fetterer, F., Savoie, M., Mallory, S., Duerr, R., and Stroeve, J.:

674 NOAA/NSIDC Climate Data Record of Passive Microwave Sea Ice Concentration.

675 Version 2, Boulder, Colorado USA: National Snow and Ice Data Center,

676 http://dx.doi.org/10.7265/N55M63M1, 2013.

677 Moore, T. S., Dowell, M. D., and Franz, B. A.: Detection of coccolithophore blooms in

678 ocean color satellite imagery: A generalized approach for use with multiple sensors,

679 Rem. Sens. Env., 117, 249–263, doi: 10.1016/j.rse.2011.10.001, 2012.

680 Mucci, A., Lansard, B., Miller, L. A., and Papakyriakou, T. N.: $CO_2$ fluxes across the

681 air-sea interface in the southeastern Beaufort Sea: Ice-free period, J. Geophys. Res.,

682 115, C04003, doi:10.1029/2009JC005330, 2010.

683 Murata, A.: Increased surface seawater $pCO_2$ in the eastern Bering Sea shelf: An effect

684    of blooms of coccolithophorid *Emiliania huxleyi*? Global Biogeochem. Cycles, 20,

685    GB4006, doi:10.1029/2005GB002615, 2006.

686    Murray, F. W.: On the computation of saturation vapor pressure. J. Applied Meteorology,

687    6, 203–204, 1967.

688    Nakaoka, S., Telszewski, M., Nojiri, Y., Yasunaka, S., Miyazaki, C., Mukai, H., and

689    Usui, N.: Estimating temporal and spatial variation of sea surface $pCO_2$ in the North

690    Pacific using a self organizing map neural network technique, Biogeosciences, 10,

691    6093-6106, doi:10.5194/bg-10-6093-2013, 2013.

692    Olsen, A., Brown, K. R., Chierici, M., Johannessen, T., and Neill, C.: Sea-surface $CO_2$

693    fugacity in the subpolar North Atlantic, Biogeosciences, 5, 535–547,

694    doi:10.5194/bg-5-535-2008, 2008.

695    Olsen, A., Key, R. M., van Heuven, S., Lauvset, S. K., Velo, A., Lin, X., Schirnick, C.,

696    Kozyr, A., Tanhua, T., Hoppema, M., Jutterström, S., Steinfeldt, R., Jeansson, E.,

697    Ishii, M., Pérez, F. F., and Suzuki, T.: The Global Ocean Data Analysis Project

698    version 2 (GLODAPv2) – an internally consistent data product for the world ocean,

699    Earth Syst. Sci. Data, 8, 297–323, 2016, doi:10.5194/essd-8-297-2016, 2016.

700    O'Reilly, J. E., Maritorena, S., Mitchell, B. G., Siegel, D. A., Carder, K. L., Garver, S. A.,

701    Kahru, M., and McClain, C.: Ocean color chlorophyll algorithms for SeaWiFS, J.

702     Geophys. Res., 103, 24937–24953, doi:10.1029/98JC02160, 1998.

703     Peng, G., Meier, W., Scott, D., and Savoie, M.: A long-term and reproducible passive

704     microwave sea ice concentration data record for climate studies and monitoring.

705     Earth Syst. Sci. Data 5: 311–318, http://dx.doi.org/10.5194/essd-5-311-2013, 2013.

706     Perrette, M., Yool, A., Quartly, G. D., and Popova, E. E.: Near-ubiquity of ice-edge

707     blooms in the Arctic, Biogeosciences, 8, 515–524, doi:10.5194/bg-8-515-2011, 2011.

708     Reynolds, R. W., Rayner, N. A., Smith, T. M., Stokes, D. C., and Wang, W.: An

709     improved in situ and satellite SST analysis for climate, J. Climate, 15, 1609–1625,

710     2002.

711     Schuster, U., McKinley, G. A., Bates, N., Chevallier, F., Doney, S. C., Fay, A. R.,

712     González-Dávila, M., Gruber, N., Jones, S., Krijnen, J., Landschützer, P., Lefèvre, N.,

713     Manizza, M., Mathis, J., Metzl, N., Olsen, A., Rios, A. F., Rödenbeck, C.,

714     Santana-Casiano, J. M., Takahashi, T., Wanninkhof, R., and Watson, A. J.: An

715     assessment of the Atlantic and Arctic sea–air $CO_2$ fluxes, 1990–2009,

716     Biogeosciences, 10, 607–627, doi:10.5194/bg-10-607-2013, 2013.

717     Shutler, J. D., Land, P. E., Brown, C. W., Findlay, H. S., Donlon, C. J., Medland, M.,

718     Snooke, R., and Blackford, J. C.: Coccolithophore surface distributions in the North

719     Atlantic and their modulation of the air-sea flux of $CO_2$ from 10 years of satellite

720    Earth observation data, Biogeosciences, 10, 2699–2709,

721    doi:10.5194/bg-10-2699-2013, 2013

722    Semiletov, I., Makshtas, A., Akasofu, S.-I., and Andreas, E. L: Atmospheric $CO_2$

723    balance: The role of Arctic sea ice, Geophys. Res. Lett., 31, L05121,

724    doi:10.1029/2003GL017996, 2004.

725    Semiletov, I. P., Pipko, I. I., Repina, I., and Shakhova, N. E.: Carbonate chemistry

726    dynamics and carbon dioxide fluxes across the atmosphere–ice–water interfaces in

727    the Arctic Ocean: Pacific sector of the Arctic, Journal of Marine Systems, 66, 204–

728    226, doi:10.1016/j.jmarsys.2006.05.012, 2007.

729    Signorini, S. R., and McClain, C. R.: Effect of uncertainties in climatologic wind, ocean

730    $pCO_2$, and gas transfer algorithms on the estimate of global sea-air $CO_2$ flux, Global

731    Biogeochem. Cycles, 23, GB2025, doi:10.1029/2008GB003246, 2009.

732    Siswanto, E., Tang, J., Ahn, Y.-H., Ishizaka, J., Yoo, S., Kim, S.-W., Kiyomoto, Y.,

733    Yamada, K., Chiang, C., and Kawamura, H.: Empirical ocean color algorithms to

734    retrieve chlorophyll-a, total suspended matter, and colored dissolved organic matter

735    absorption coefficient in the Yellow and East China Seas, Journal of Oceanography,

736    doi:10.1007/s10872-011-0062-z, 2011.

737    Siswanto, E., Ishizaka, J., Tripathy, S. C., and Miyamura, K.: Detection of harmful algal

738    blooms of *Karenia mikimotoi* using MODIS measurements: a case study of

739    Seto-Inland Sea, Japan, Remote Sensing of Environment, 129, 185–196,

740    doi:10.1016/j.rse.2012.11.003, 2013.

741    Smyth, T. J., Tyrrell, T., Tarrant, B.: Time series of coccolithophore activity in the

742    Barents Sea, from twenty years of satellite imagery, Geophys. Res. Lett., 31, L11302,

743    doi:10.1029/2004GL019735, 2004.

744    Steele, M., Morley, R., and Ermold, W.: PHC: A global ocean hydrography with a high

745    quality Arctic Ocean, J. Climate, 14, 2079–2087, 2001.

746    Sweeney, C., Gloor, E., Jacobson, A. R., Key, R. M., McKinley, G., Sarmiento, J. L.,

747    and Wanninkhof, R.: Constraining global air-sea gas exchange for $CO_2$ with recent

748    bomb $^{14}C$ measurements, Global Biogeochem. Cycles, 21, GB2015,

749    doi:10.1029/2006GB002784, 2007.

750    Takahashi, T., Sutherland, S. C., Wanninkhof, R., Sweeney, C., Feely, R. A., Chipman,

751    D. W., Hales, B., Friederich, G., Chavez, F., Sabine, C., Watson, A., Bakker, D. C. E.,

752    Schuster, U., Metzl, N., Yoshikawa-Inoue, H., Ishii, M., Midorikawa, T., Nojiri, Y.,

753    Körtzinger, A., Steinhoff, T., Hoppema, M., Olafsson, J., Arnarson, T. S., Tilbrook,

754    B., Johannessen, T., Olsen, A., Bellerby, R., Wong, C. S., Delille, B., Bates, N. R., de

755    Baar, H. J. W.: Climatological mean and decadal changes in surface ocean $pCO_2$, and

756     net sea-air $CO_2$ flux over the global oceans. Deep-Sea Res. II, 56, 554–577, 2009.

757     Takahashi, T., Sutherland, S.C., and Kozyr, A.: Global Ocean Surface Water Partial

758     Pressure of $CO_2$ Database: Measurements Performed During 1957–2014 (Version

759     2014). ORNL/CDIAC-160, NDP-088(V2014). Carbon Dioxide Information Analysis

760     Center, Oak Ridge National Laboratory, U.S. Department of Energy, Oak Ridge,

761     Tennessee, doi: 10.3334/CDIAC/OTG.NDP088(V2014), 2015.

762     Tassan, S.: Local algorithms using SeaWiFS data for the retrieval of phytoplankton,

763     pigments, suspended sediment, and yellow substance in coastal waters, Appl Opt., 33,

764     2369–2378, doi:10.1364/AO.33.002369, 1994.

765     Telszewski, M., Chazottes, A., Schuster, U., Watson, A. J., Moulin, C., Bakker, D.C.E.,

766     González-Dávila, M., Johannessen, T., Körtzinger, A., Lüger, H., Olsen, A., Omar, A.,

767     Padin, X. A., Ríos, A. F., Steinhoff, T., Santana-Casiano, M., Wallace, D. W. R., and

768     Wanninkhof, R.: Estimating the monthly $pCO_2$ distribution in the North Atlantic

769     using a self-organizing neural network, Biogeosciences, 6, 1405–1421,

770     doi:10.5194/bg-6-1405-2009, 2009.

771     Ulfsbo, A., Cassar, N., Korhonen, M., van Heuven, S., Hoppema, M., Kattner, G., and G.

772     Anderson, L.: Late summer net community production in the central Arctic Ocean

773     using multiple approaches, Global Biogeochem. Cycles, 28, 1129–1148,

774     doi:10.1002/2014GB004833, 2014.

775     van Heuven, S., Pierrot, D., Lewis, E., and Wallace, D. W. R.: MATLAB Program

776         Developed for CO2 System Calculations, ORNL/CDIAC-105b. Carbon Dioxide

777         Information Analysis Center, Oak Ridge National Laboratory, US Department of

778         Energy, Oak Ridge, Tennessee, 2009.

779     Wanninkhof, R.: Relationship between wind speed and gas exchange over the ocean, J.

780         Geophys. Res., 97(C5), 7373–7382, doi:10.1029/92JC00188, 1992.

781     Wanninkhof, R., Park, G. -H., Takahashi, T., Sweeney, C., Feely, R., Nojiri, Y., Gruber,

782         N., Doney, S. C., McKinley, G. A., Lenton, A., Le Quéré, C., Heinze, C., Schwinger,

783         J., Graven, H., and Khatiwala, S.: Global ocean carbon uptake: magnitude, variability

784         and trends, Biogeosciences, 10, 1983–2000, doi:10.5194/bg-10-1983-2013, 2013.

785     Wanninkhof, R.: Relationship between wind speed and gas exchange over the ocean

786         revisited, Limnology and Oceanography: Methods, 12, 351-362, 2014.

787     Weiss, R. F.: Carbon dioxide in water and seawater: the solubility of a non-ideal gas,

788         Marine Chemistry, 2, 203–215, 1974.

789     Yasunaka, S., Nojiri, Y., Nakaoka, S., Ono, T., Whitney, F. A., and Telszewski, M.:

790         Mapping of sea surface nutrients in the North Pacific: Basin-wide distribution and

791         seasonal to interannual variability, J. Geophys. Res. Oceans, 119, 7756–7771,

792     doi:10.1002/2014JC010318, 2014.

793     Yasunaka, S., Murata, A., Watanabe, E., Chierici, M., Fransson, A., van Heuven, S.,

794     Hoppema, M., Ishii, M., Johannessen, T., Kosugi, N., Lauvset, S. K., Mathis, J. T.,

795     Nishino, S., Omar, A. M., Olsen, A., Sasano, D., Takahashi, T., and Wanninkhof, R.:

796     Mapping of the air–sea $CO_2$ flux in the Arctic Ocean and its adjacent seas:

797     basin-wide distribution and seasonal to interannual variability, Polar Science, 10,

798     323–334, doi:10.1016/j.polar.2016.03.006, 2016.

Figure 1: Map of the Arctic Ocean and its adjacent seas. Gray contour lines show the 1000, 2000, 3000, and 4000 m isobaths. Blue lines show the 17-year annual mean position of the ice edge (SIC = 15 %). Area for the mapping is north of 60° N (heavy black circle). Sectors selected for regional analysis are the Arctic Ocean (dashed magenta line), the Greenland/Norwegian Seas (green 1), the Barents Sea (green 2), and the Chukchi Sea (green 3).
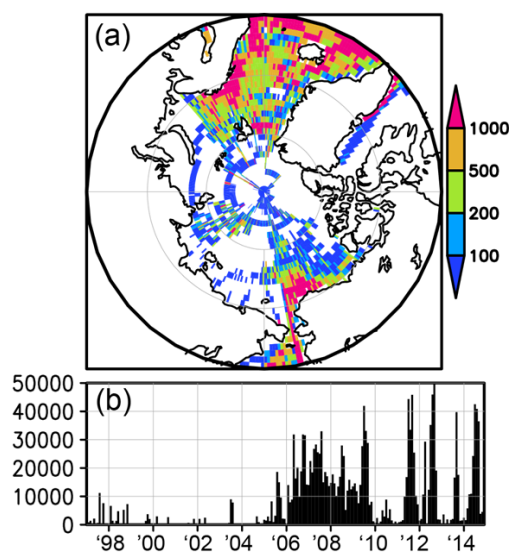
Figure 2: (a) The number of ocean surface $CO_2$ data in the grid boxes (1° × 1°) used in

this study. Data are from SOCATv4, LDEOv2014, GLODAPv2, and collected by R/V

*Mirai* of JAMSTEC between 1997 and 2014. (b) Monthly time series of the number of

$CO_2$ data in the analysis area (north of 60° N).
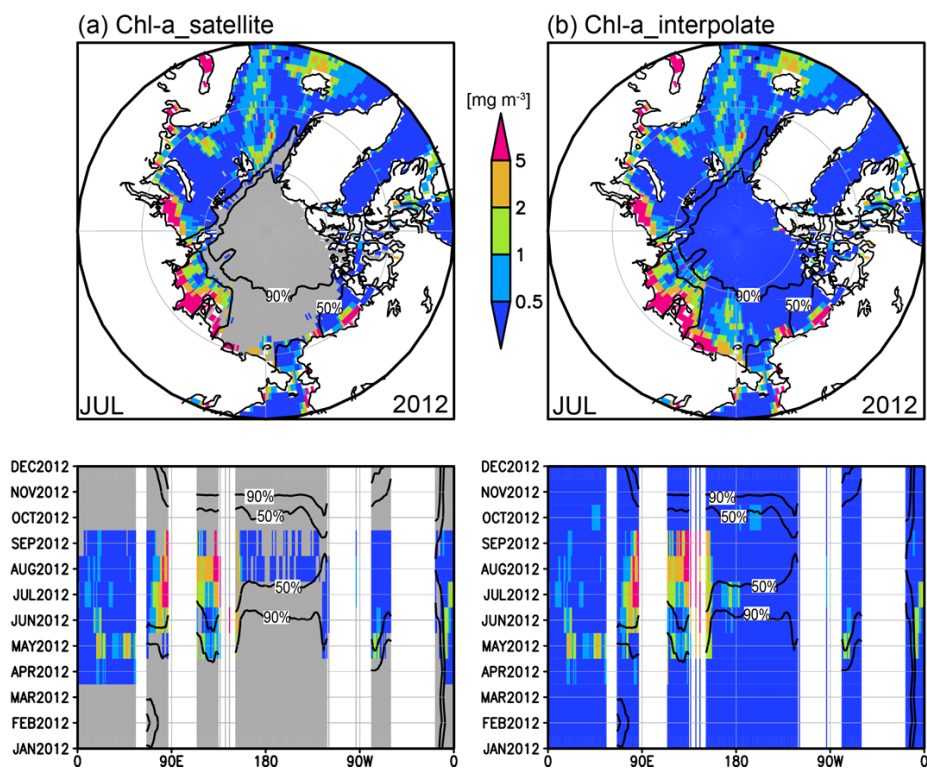
Figure 3: (a) Original and (b) interpolated Chl-a [mg m$^{-3}$] in July 2012 (upper panels),

and along 75°N in 2012 (lower panels). Black lines denote SIC of 50% and 90%. Gray

areas in (a) indicate missing Chl-a data.
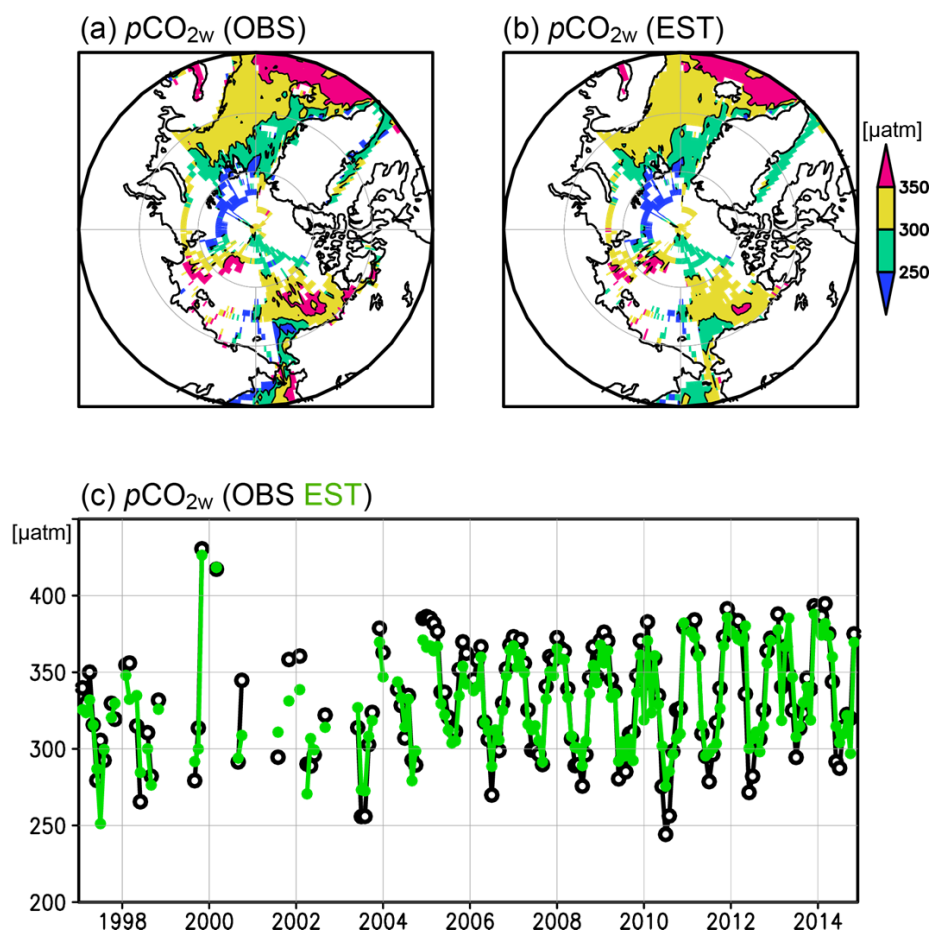
Figure 4: (a) Observed $pCO_{2w}$ averaged over the whole analysis period [µatm]. (b)

Estimated $pCO_{2w}$ averaged over the grid boxes in which observed $pCO_{2w}$ values were

available [µatm]. (c) Monthly time series of observed $pCO_{2w}$ averaged over the entire

analysis area (black), and estimated $pCO_{2w}$ averaged over the grid boxes in which

observed $pCO_{2w}$ values were available (green) [µatm].
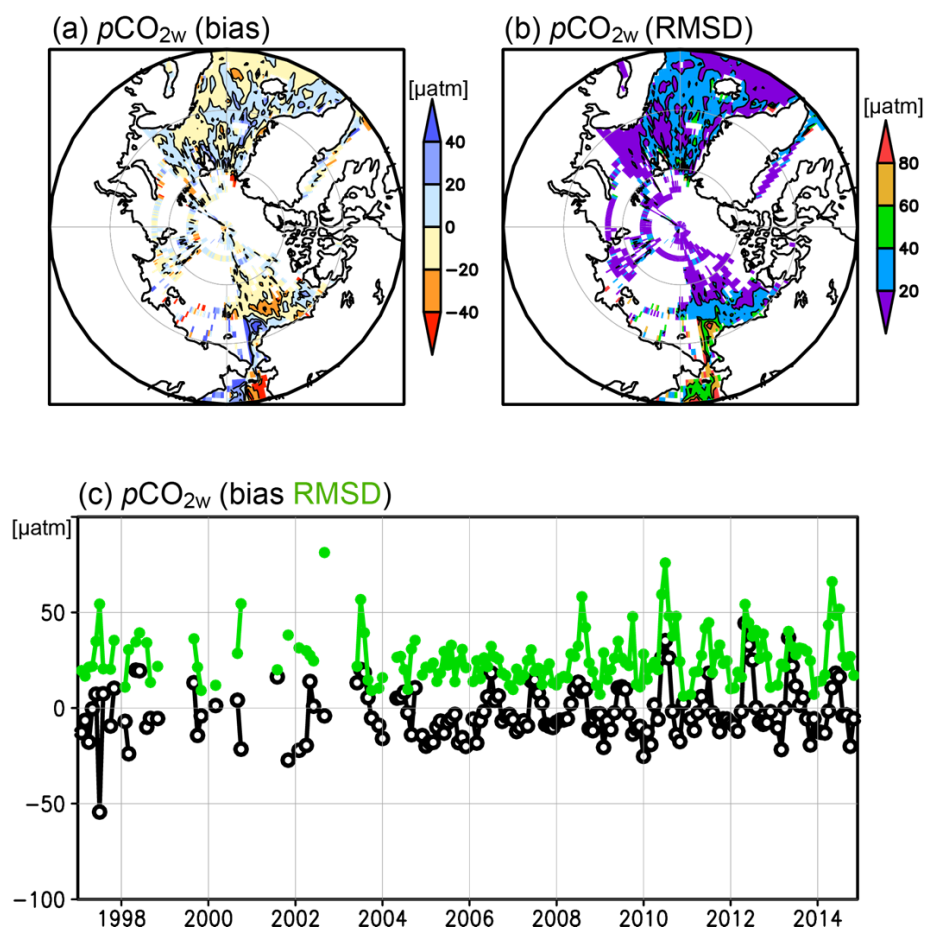
Figure 5: (a) Bias (estimate–observation) and (b) root-mean-square-difference between

observed and estimated $pCO_{2w}$ averaged over the whole analysis period [µatm]. (c) Bias

(estimate–observation; black) and root-mean-square-difference (green) between

observed and estimated $pCO_{2w}$ averaged over the entire analysis area [µatm].
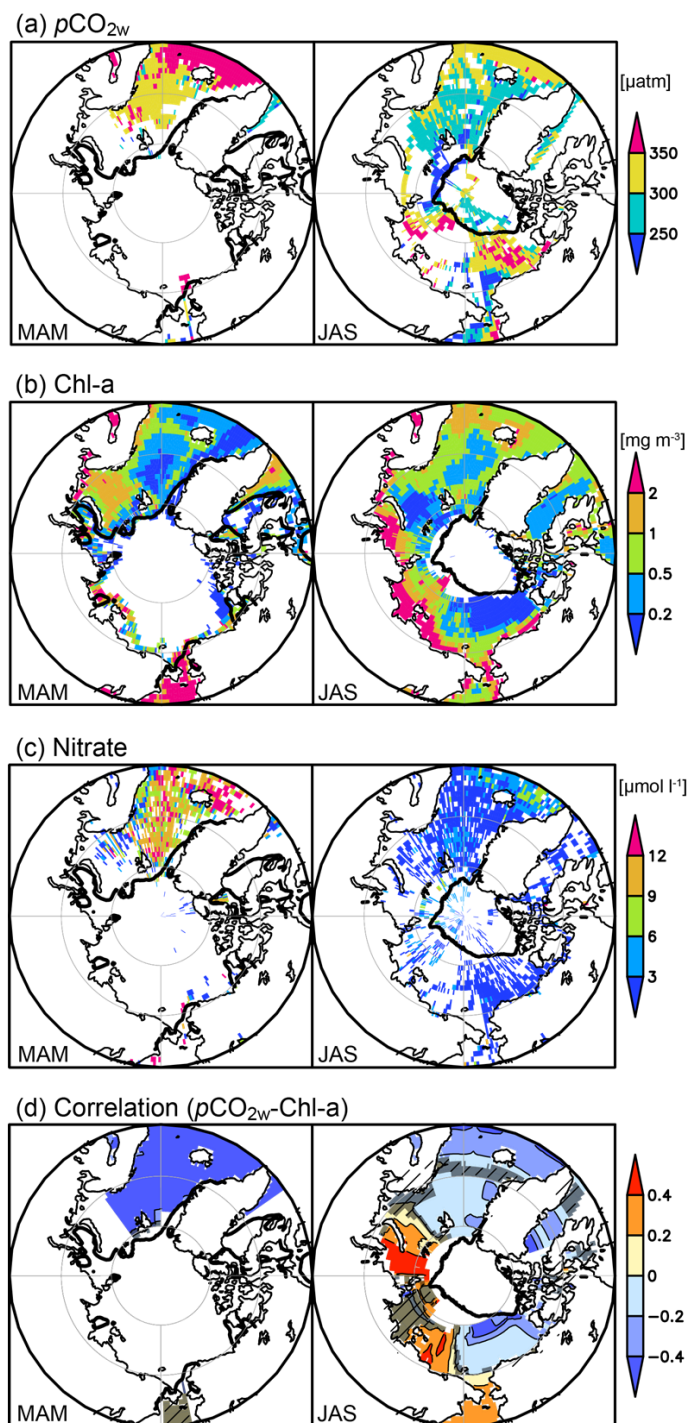
Figure 6: (a) Observed $pCO_{2w}$ [µatm], (b) non-interpolated Chl-a [mg m$^{-3}$] and (c) surface nitrate concentration [µmol l$^{-1}$] in March–May (left), and July–September (right) from 1997 to 2014. (d) Spatial correlation (correlation coefficient, $r$) between $pCO_{2w}$ and Chl-a in a window size of ±1 month, ±5° of latitude, and ±30° of longitude in March–May (left), and July–September (right). Darker hatched areas represent values in grids where correlations are insignificant ($P > 0.05$).
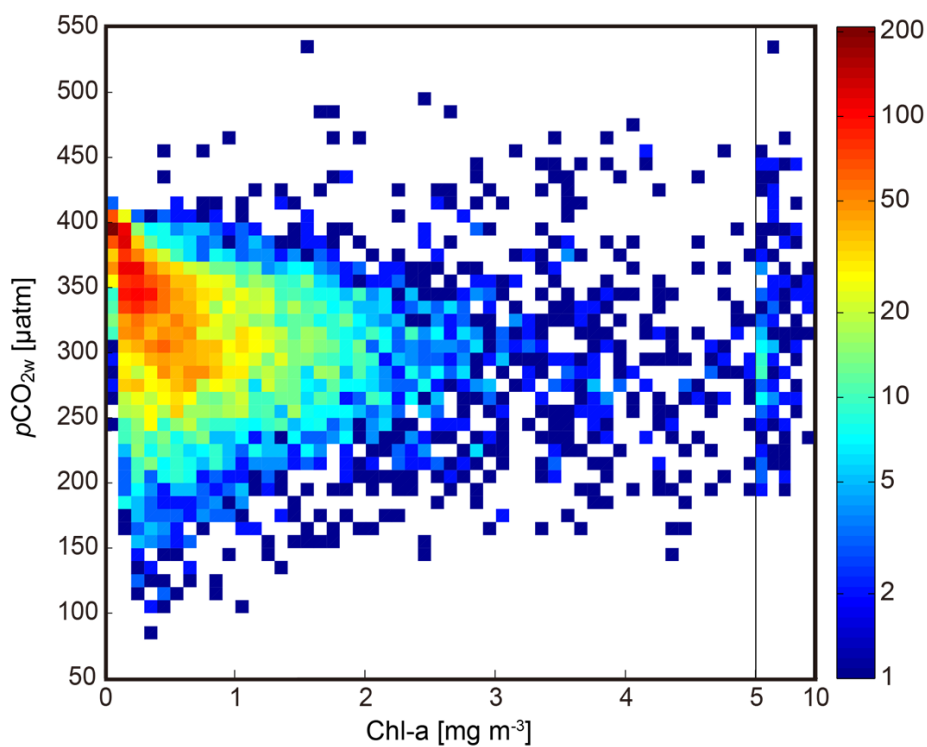
Figure 7: Observed $pCO_{2w}$ [μatm] vs. satellite Chl-a [mg m$^{-3}$] in the Arctic Ocean and

its adjacent seas (north of 60° N) from 1997 to 2014. Colors indicate the number of data

pairs in a 0.1 mg m$^{-3}$ × 5 μatm bin when Chl-a ≤ 5 mg m$^{-3}$, or in a 1 mg m$^{-3}$ × 5 μatm

bin when Chl-a > 5 mg m$^{-3}$.
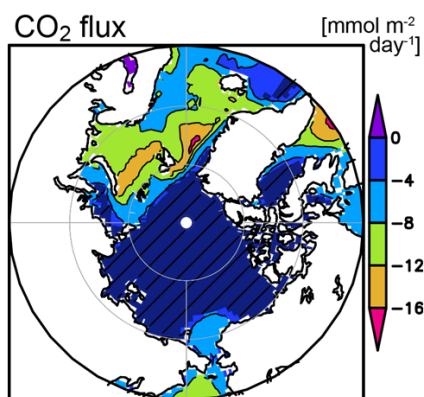
Figure 8: Eighteen-year annual means of $CO_2$ flux [mmol m$^{-2}$ day$^{-1}$] (negative values

indicate flux into the ocean). Darker hatched areas represent show values in grids where

fluxes were smaller than the uncertainty, estimated as described in the text.
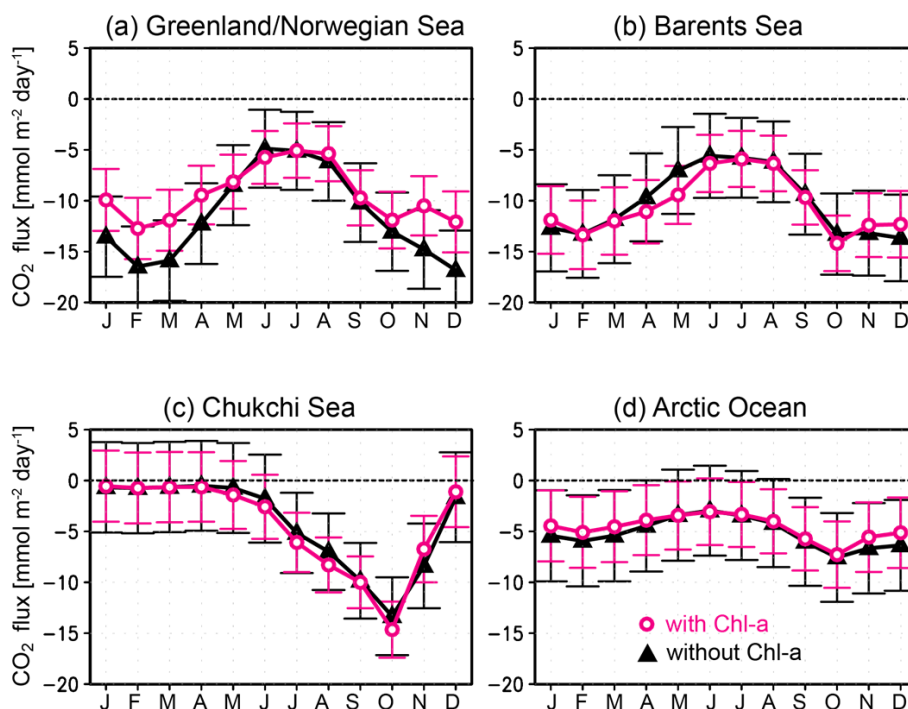
Figure 9: Eighteen-year monthly mean $CO_2$ flux [mmol m$^{-2}$ day$^{-1}$] averaged over (a) the

Greenland/Norwegian Seas, (b) the Barents Sea, (c) the Chukchi Sea, and (d) the Arctic

Ocean. Black lines with triangles show estimates without Chl-a by Yasunaka et al.

(2016); magenta lines with open circles show estimates with Chl-a. Error bars show the

uncertainty, estimated as described in the text.
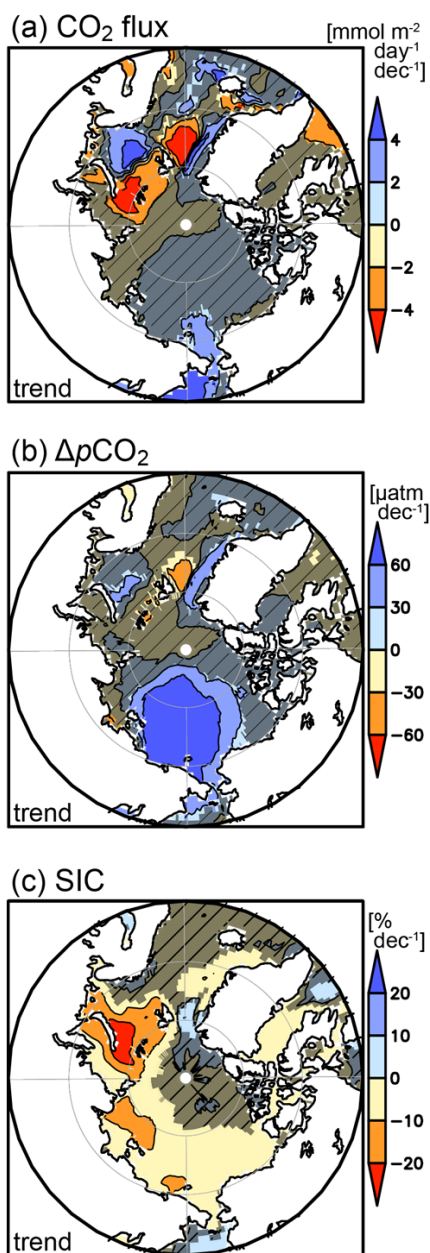
Figure 10: Trends in (a) $CO_2$ flux [mmol m$^{-2}$ day$^{-1}$ decade$^{-1}$], (b) $\Delta p CO_2$ [μatm decade$^{-1}$], and (c) SIC [% decade$^{-1}$]. Darker hatched areas represent values in grids where trend values were less than the uncertainty, estimated as described in the text.
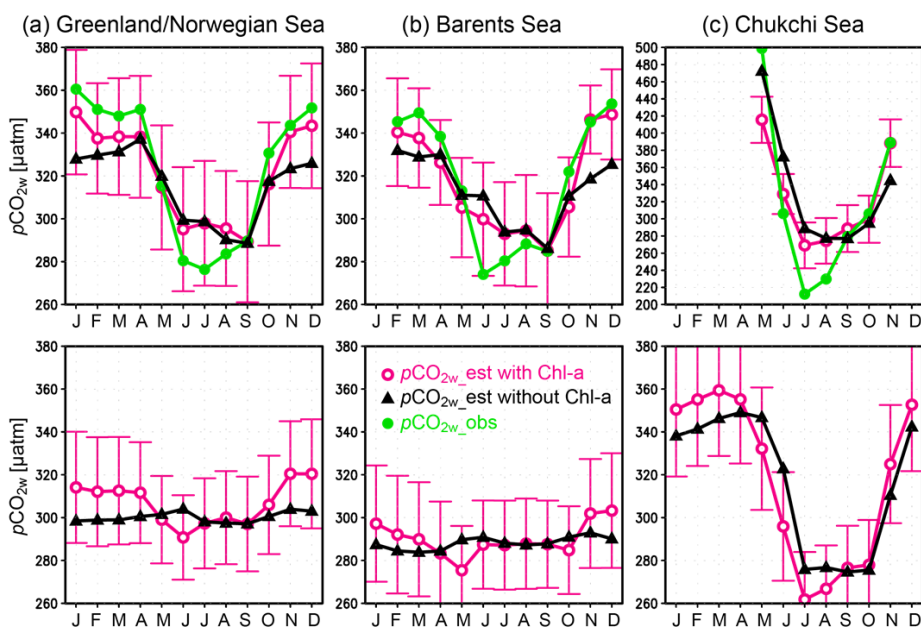
Figure 11: Eighteen-year averaged $p$CO$_{2w}$ seasonal variations [µatm] in (a) the

Greenland/Norwegian Seas, (b) the Barents Sea, and (c) the Chukchi Sea. Black lines

with triangles show estimates without Chl-a; magenta lines with open circles show

estimates with Chl-a; green lines with closed circles show observed values. The upper

panels show $p$CO$_{2w}$ averaged over the grid boxes in which observed $p$CO$_{2w}$ values were

available, and the lower panels show $p$CO$_{2w}$ averaged for all grid cells with each region.

Error bars show the uncertainty, estimated as described in the text.

Table 1: RMSD [mg m$^{-3}$] and correlation ($r$) between Chl-a values

|  | standard algorithm | | coastal algorithm | |
| --- | --- | --- | --- | --- |
|  | RMSD | $r$ | RMSD | $r$ |
| Chl-a from Arctic algorithm | 0.80 | 0.90 | 0.81 | 0.87 |
| Interpolated Chl-a from Arctic algorithm | 0.37 | 0.92 | 0.48 | 0.86 |